World Applied Sciences Journal 6 (7): 914-925, 2009
ISSN 1818-4952
© IDOSI Publications, 2009

Modeling of a Novel High-*Q*, Highly Linear, IF Micromechanical Filter: Design and Simulations

Farshad Babazadeh and Sayyed-Hossein Keshmiri

Department of Electrical Engineering, Faculty of Engineering,
Ferdowsi University, Mashhad, 91775-1111, Iran

Abstarct: In this paper, design and simulation of a novel IC-compatible microelectromechanical bandpass filter for use in intermediate frequency range of a wireless communication system is reported. This filter is composed of two high-*Q* square frame microresonators coupled by a soft flexural-mode mechanical spring and can be implemented using either thick epitaxial polysilicon technology or bulk micromachining of SOI wafers. The resonators with new design and structure determine the center frequency, while a mechanical coupling spring defines the bandwidth of the filter. Quarter-wavelength coupling is required on this microscale to alleviate mass-loading effects caused by similar resonator and coupler dimensions. Filter center frequencies around 72 MHz, 285 kHz bandwidth, quality factor of 250, associated insertion loss less than 0.44 dB, spurious-free dynamic ranges around 99 dB and input and output termination resistances on the order of 9 kΩ were obtained by this design.

Key words: Bandpass filter . motional resistance . micromechanical resonator . quality factor . MEMS

INTRODUCTION

Miniaturization of the constituent components of super-heterodyne wireless transceivers is a field of research that has received considerable attention recently. Reduced size constitutes the most obvious incentive for replacing SAWs and crystals by equivalent devices. Typically, the front-end of a wireless transceiver contains a good number of off-chip high-*Q* components that are potentially replaceable by micromechanical versions. Among the components targeted for replacement are RF filters, including image reject filters, IF filters and high-*Q* low phase-noise local oscillators [1-3]. One of the challenging issues which has hindered deployment of the microelectromechanical resonators and filters is large motional resistance R_x of these devices with electrostatically and capacitively transduction.

Among methods for lowering the motional resistance R_x of electrostatically and capacitively transduced micromechanical resonators presented so far are: 1) decreasing the electrode-to-resonator gap [4], 2) increasing the dc-bias voltage V_{DC} and 3) summing together the output currents of an array of identical resonators [5]. Unfortunately, each of these methods comes with some drawbacks. In particular, although the first two methods are very effective in lowering R_x (with fourth power and square law dependencies, respectively), they do so at the cost of linearity [6, 7]. On the other hand, method (3) actually improves linearity while lowering R_x. However, this method is difficult to implement; since it requires resonators with precisely identical responses and consumes large area of silicon chip; since it uses an array of resonators instead of a single resonator.

This paper presents a novel method for lowering motional resistance based on a technique which utilizes true potential of a single square frame resonator in three-dimensions and raises the linearity as well. Using this new technique, a bandpass filter composed of two square frame resonators (with an effective R_x of 478 Ω) was designed and simulated at 72 MHz. This effective resistance is about 75X smaller than the 35.9 kΩ exhibited by a 72 MHz Clamped-Clamped (CC) beam resonator [8], 73X smaller than the 34.8 kΩ demonstrated by a 71 MHz Free-Free (FF) beam resonator [9] and 8.4X smaller than the 4kΩ presented by a 68.1 MHz mechanically-coupled 11-resonators array [5].

This R_x-reduction method is superior to methods based on scaling down of electrode-to-resonator gaps, dc-bias increases, or using an array of identical resonators; because it allows a reduction in R_x without sacrificing linearity and consuming large chip area. Furthermore, achievable quality factor of the proposed resonator is almost an order of magnitude higher than

Corresponding Author: Dr. Farshad Babazadeh, Department of Electrical Engineering, Faculty of Engineering, Ferdowsi University, Mashhad, 91775-1111, Iran

that of a 71 MHz Clamped-Clamped beam resonator. Also, realization of a microfilter by coupling two or more square frame resonators is much simpler than coupling some Free-Free beam resonators.

MATERIALS AND METHODS

Filter structure and operation: Figure 1 shows schematic top view of a two-resonator filter (along with bias voltage, excitation and sensing circuitry). This filter consists of two identical micromechanical square frame resonators, coupled mechanically by a flexural-mode beam, all suspended above the substrate. The structure is supported by four tethers and attached to substrate only at anchors.

To operate this filter, a dc-bias V_{DC} is applied to the suspended filter structure and two equal and opposite *ac* voltages v_i and-v_i are applied through R_{Q11} and R_{Q12} resistors to the input electrodes, which are placed by a 100 nm gap from the structure, as shown in Fig. 1. The application of input voltages v_i and-v_i create *x*-and *y*-directed electrostatic forces between input electrodes and the conductive resonator that induce *x*-and *y*-directed vibration of the input resonator when the frequency of the input voltages come within the passband of the mechanical filter. This vibrational energy is transferred to the output resonator via the coupling spring, causing it to vibrate as well. Vibration of the output resonator creates some dc-biased, time-varying capacitors between the conductive resonator and output electrodes, which then source two output currents given by:

$$i_{o1} = 2V_{DC}\left(\frac{\partial C_{in}}{\partial x}\frac{\partial x}{\partial t} + \frac{\partial C_{out}}{\partial y}\frac{\partial y}{\partial t}\right)$$
$$i_{o2} = -2V_{DC}\left(\frac{\partial C_{in}}{\partial y}\frac{\partial y}{\partial t} + \frac{\partial C_{out}}{\partial x}\frac{\partial x}{\partial t}\right) \quad (1)$$

where $\partial C_{in}/\partial x$, $\partial C_{in}/\partial y$, $\partial C_{out}/\partial x$ and $\partial C_{out}/\partial y$ are the changes in resonator-to-inner electrodes and resonator-to-outer electrodes capacitances per unit displacement at output ports in *x* and *y* directions, respectively. The output currents i_{o1} and i_{o2} are then directed to resistors R_{Q21} and R_{Q22}, which convert the currents to output voltages and provide the proper termination impedance required to flatten the jagged passband.

The basis of operation of two-resonator mechanical filter is shown in Fig. 2. Such a coupled two-resonator system exhibits two mechanical resonance modes with closely spaced frequencies that define the filter passband. The center frequency of the filter is determined primarily by the frequencies of the

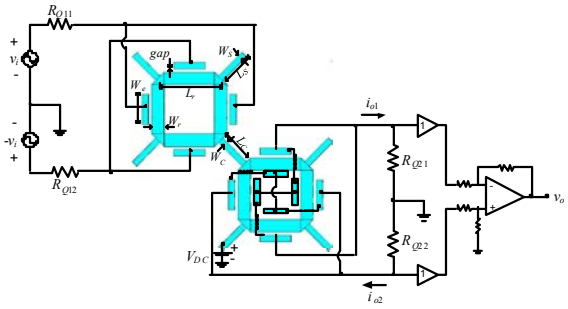

Fig. 1: Top view schematic of a two-resonator micromechanical filter, along with the bias voltage, excitation and sensing circuitry. (Inner Electrodes for the input resonator are not shown for simplicity)

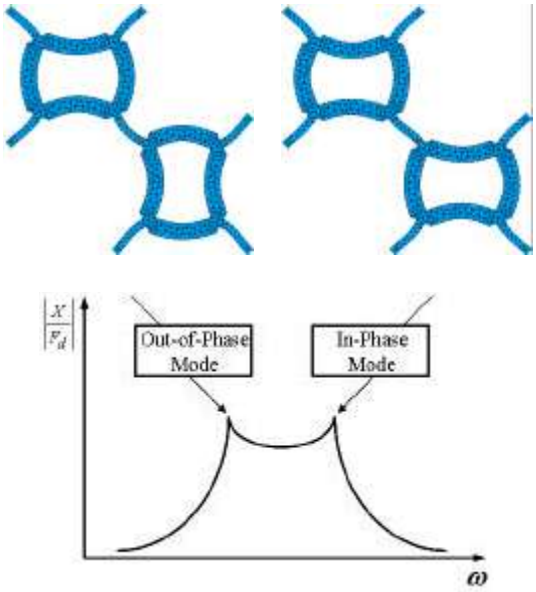

Fig. 2: Filter mode shapes and their correspondence to specific peaks in the unterminated frequency characteristic

constituent resonators, while the spacing between modes (i.e., the bandwidth) is determined largely by the stiffness of the coupling spring. As shown in Fig. 2, each mode peak corresponds to a distinct, physical mode shape. In the lower frequency mode, both resonators vibrate in phase and in the higher frequency mode, the resonators are 180 degrees out of phase.

Design of the micromechanical resonator in form of Fig. 3, has some advantages as follows:

- The fully-differential electrode configuration cancels the second harmonic distortion term (HD_2); therefore, improving the power-handling capability and dynamic range of the filter.

- The present structure design, decreases input and output impedances significantly and matches the impedance of filter to the impedances of the stages before and after the filter, properly.
- Since the proposed resonator structure has four almost motionless node points, the quality factor due to energy loss mechanisms of support loss ($Q_{Support}$) is high and hence Q of the whole structure is high.
- Since the constituent resonators of the filter vibrate in x and y directions and have no motions in z direction (out-of-plane), the electrodes are placed besides the structure instead of beneath it. So, the fabrication, mask defining, pattern generation and manufacturing of the device will be done more easily and inexpensively.
- Although, the square frame resonator can be supposed as four electrically coupled simply-supported beam resonators vibrating at their fundamental flexural-mode resonant frequencies, which essentially are not the same due to fabrication tolerances, however, the proposed square frame resonator vibrates only at single frequency, even if dimensions of the constituent beams of the frame be unequal.

Generally, the design of the proposed micromechanical filter can be summarized into following major steps:

- Design of a square frame resonator capable to resonate at the desired frequency by proper choice of dimensions.
- Estimating quality factor of the designed microresonator and choosing proper values of support beam dimensions.
- Choosing manufacturable values of coupling beam widths, dictated predominantly by lithographic and etch resolution.
- Design of flexural mode coupling beam lengths to correspond to effective quarter-wavelenghts of the filter centre frequency and evaluate the resulting stiffnesses of the coupling beam in cases of two physical mode shapes.
- Choosing bandwidth of the filter and achieving thickness of the coupling beam.
- Determining the motional resistance of the microresonator, desired values of filter termination resistances and insertion loss of the filter.
- Estimating linearity of the filter by calculating spurious-free dynamic range criterion.

Each of the above steps will be discussed in the following subsections.

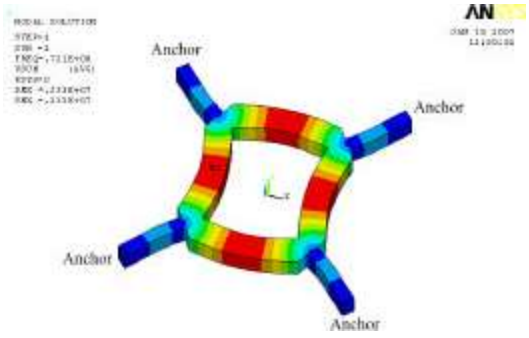

Fig. 3: Fundamental mode shape of the micromechanical resonator simulated by ANSYS

Qualitative description of resonator structure: Since center frequency of a given mechanical filter is determined primarily by the resonance frequencies of its constituent resonators, careful mechanical resonator design is imperative for successful filter implementation. The selected resonator design must not only be able to achieve the needed frequency but must also do so with adequate linearity and tunability and with sufficient Q.

As shown in Fig. 3, the microresonator is formed of four polysilicon beams which are attached to each other and organized in a square frame. Other polysilicon tethers attach corners of this frame to anchors. The anchors are tightly placed on substrate and caused the whole structure to suspend above the substrate with a little space between them. This polysilicon square frame can freely move parallel to substrate in x and y orientations.

The resonance frequency of this simply-supported square frame depends upon many factors, including geometry, structural material properties, stress, the magnitude of the applied dc-bias voltage V_{DC} and surface topography. Accounting for these while neglecting finite width effects, an expression for resonance frequency can be written as [10]:

$$f_0 = \frac{\beta_n^2}{4\pi\sqrt{3}} \kappa \frac{W_r}{L_r^2} \sqrt{\frac{E}{\rho}} \qquad (2)$$

where W_r and L_r are the width and effective length of the beam respectively, E is the Young's modulus, ρ is the density of the structural material, β_n = 3.1415, 6.2831, 9.4247 for the first three modes of a simply-supported beam, f_0 is the nominal mechanical resonance frequency of the resonator if there were no electrodes or applied voltages and κ is a scaling factor that models the effects of surface topography.

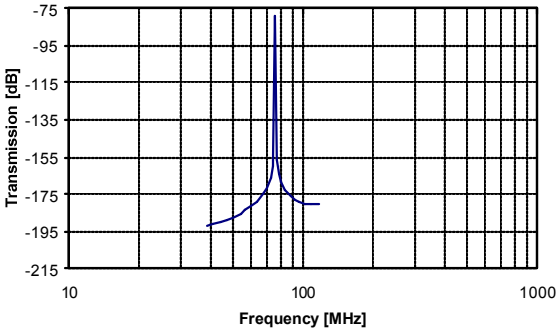

Fig. 4: Mechanical frequency response of the microresonator

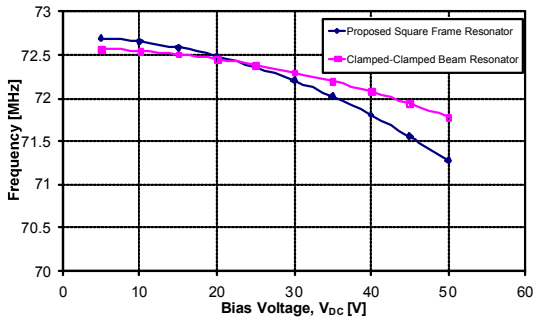

Fig. 5: Simulated frequency versus applied dc-bias V_{DC} for the present and a CC beam microresonator

Mechanical frequency response of the designed resonator is shown in Fig. 4.

To properly excite this device, a dc-bias voltage V_{DC} and two *ac* excitation voltages v_i and-v_i are applied across the input resonator-to-electrode capacitors (i.e., the input transducers). This creates a force component between the electrode and resonator proportional to the product $V_{DC}v_i$ and at the frequency of v_i. When the frequency of v_i nears its resonance frequency, the microresonator begins to vibrate, creating dc-biased time-varying capacitors $C_0(x,t)$ at the output transducers. A current is then generated through the output transducers and serve as the outputs of this device. When plotted against the frequency of the excitation signal v_i, the output currents i_{o1} and i_{o2} trace out the bandpass biquad characteristic expected for a high-Q tank circuit.

Frequency tuning: Resonance frequency of the microresonator is a function of the dc-bias voltage V_{DC}. Thus, frequency of this device is tunable via adjustment of V_{DC} and this can be used advantageously to implement filters with tunable center frequencies, or to correct for passband distortion caused by finite planar fabrication tolerances.

The dc-bias dependence of resonance frequency arises from a V_{DC}-dependent electrical spring constant k_{elec} that subtracts from the mechanical spring constant of the system k_{mech}, lowering the overall spring stiffness k_r=k_{mech}-k_{elec}, thus lowering the resonance frequency according to the expression:

$$f_0 = \frac{1}{2\pi}\sqrt{\frac{k_r}{m_r}} = \frac{1}{2\pi}\sqrt{\frac{k_{mech} - k_{elec}}{m_r}} \qquad (3)$$

where k_{mech} and m_r denote values at a particular location (usually the beam center location). Since there are two electrodes on the both sides of each constituent beam of the square frame resonator, the quantity k_{elec} is obtained as follows [11]:

$$k_{elec} = -\frac{V_{DC}^2 C_{in}}{d_0^2} - \frac{V_{DC}^2 C_{out}}{d_0^2} \qquad (4)$$

where C_{in} and C_{out} are inner electrode-to-resonator and outer electrode-to-resonator capacitances, respectively. Since it can be assumed $C_{in} \approx C_{out}$, then the quantity k_{elec} in Eq. (4) should be multiplied almost by a factor of 2. If we make a comparison between the proposed and a doubly-clamped (CC) beam resonators both resonating at the same frequency, the resonant frequency f_0 of the square frame resonator decreases further with increasing dc-bias voltage V_{DC}.

The dependence of the resonance frequency to dc-bias voltage V_{DC} for the proposed and CC beam resonators are shown in Fig. 5.

Equivalent mechanical circuit: For the purposes of filter design, it is often convenient to define an equivalent lumped-parameter mass-spring-damper mechanical circuit for this resonator (Fig. 6), with element values that vary with location on the resonator. Input parameter of this circuit is force (corresponding to voltage in electrical circuits) and the output parameter is velocity (corresponding to current). With reference to Fig. 3, the equivalent mass at a location y on the resonator is given by:

$$m_r(y) = \frac{KE_{tot}}{\frac{1}{2}v^2(y)} = \frac{\rho W_r h \int_0^{L_r} [X_{mode}(x)]^2 dx}{[X_{mode}(y)]^2} \qquad (5)$$

$$X_{mode}(y) = \sin ky \qquad (6)$$

where $k = \pi/L_r$ for the fundamental mode shape function $X_{mode}(y)$, KE_{tot} is the peak kinetic energy in the

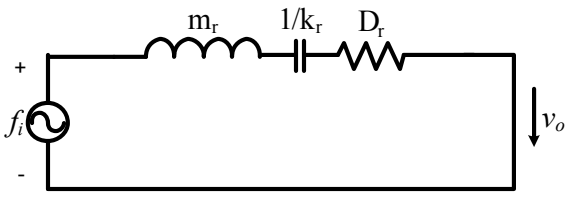

Fig. 6: Equivalent mechanical circuit for a micromechanical resonator with force f_i and velocity v_o as input and output, respectively

system, $v(y)$ is the velocity at location y and W_r and h, are width and thickness of the suspending beam, respectively. Stiffness at the middle of each constituent beam of the square frame resonator and at the coupling location were achieved by following expressions [4, 12]:

$$k_m\left(L_r/2\right) = 4Eh\left(\frac{W_r}{L_r}\right)^3 \quad (7)$$

$$k_m(y = l_c) = \frac{k_m\left(L_r/2\right)}{X^2_{mode}(y = l_c)} \quad (8)$$

The equivalent spring stiffness is given by:

$$k_r(L_r/2) = \omega_0^2 m_r(L_r/2) \quad (9)$$

where ω_0 is the angular resonance frequency of the beam. The damping factor is given by:

$$D_r(L_r/2) = \frac{\sqrt{k_m(L_r/2)\, m_r(L_r/2)}}{Q} \quad (10)$$

where Q is the quality factor of the resonator without the influence of applied voltages and electrodes.

Equivalent electrical circuit: An electrical model with a core *RLC* circuit was defined for the microresonator based on mass-spring-damper system. When looking into the electrode port of the equivalent resonator circuit of Fig. 6, a transformed *LCR* circuit is seen with element values given by:

$$L_x = \frac{m_r}{\eta_e^2} \quad , \quad C_x = \frac{\eta_e^2}{k_r} \quad , \quad R_x = \frac{\sqrt{k_r m_r}}{Q\eta_e^2} = \frac{D_r}{\eta_e^2} \quad (11)$$

where η_e is the transduction parameter for a capacitive transducer and is calculated theoretically as follows:

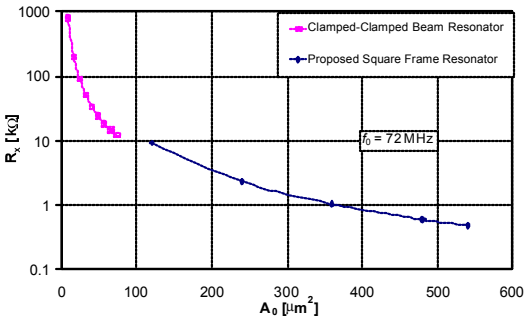

Fig. 7: Simulated plot presenting motional resistance R_x versus electrode overlap area A_0 for the proposed and a CC beam resonator

$$\eta_e = V_P\left(\frac{\partial C}{\partial x}\right) = \frac{V_{DC}\varepsilon_0 A_0}{d_0^2} \quad (12)$$

Of the elements in Eqs. (11), the series motional resistance R_x is the most influential in filter circuits. In bandpass filters, it dictates the ease of matching the designed filter to low impedance stages before and after the filter. A closed form formula for R_x is obtained by substituting Eq. (12) into Eq. (11) which yields:

$$R_x = \frac{\sqrt{k_r m_r}\, d_0^4}{Q\varepsilon_0 A_0^2 V_{DC}^2} \quad (13)$$

where A_0 is the effective electrode-to-resonator overlap area of the resonator. From Eq. (13), for a given Q, R_x is lowered by increasing the overlap area, A_0. Fig. 7 compares R_x versus electrode-to-resonator overlap area for the square frame resonator and a CC beam resonator vibrating at the same frequency.

Support structure design: As discussed in Section 3, the designed square frame mechanical resonator is supported by four flexural beams attached at its fundamental-mode node points, (Fig. 3). Since these beams are attached at node points, the support springs sustain no translational movement during resonator vibration (ideally) and, thus, support (i.e., anchor) losses due to translational movements are greatly alleviated. Furthermore, with the recognition that the supporting flexural beams actually behave like acoustic transmission lines at the VHF frequencies of interest, flexural loss mechanisms can also be negated by strategically choosing support dimensions so that they present virtually no impedance to the simply supported beam. In particular, by choosing the dimensions of a flexural support beam such that they correspond to an

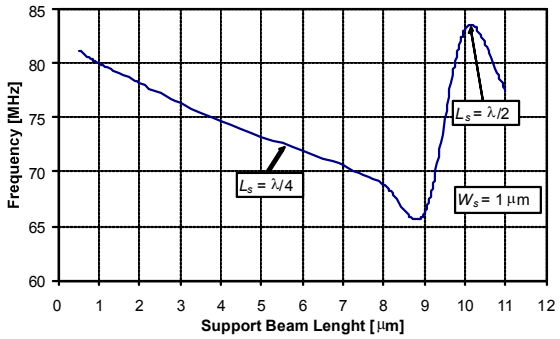

Fig. 8: Resonant frequency versus support beam length for the square frame resonator

effective quarter-wavelength of the resonator operating frequency, the solid anchor condition on one side of the support beam is transformed to a free-end condition on the other side, which connects to the resonator. In terms of impedance, the infinite acoustic impedance at the anchors is transformed to zero impedance at the resonator attachment points. As a result, the resonator effectively "sees" no supports at all and operates as if levitated above the substrate, devoid of anchors and their associated loss mechanisms.

Through appropriate acoustical network analysis, the dimensions of a flexural beam are found to correspond to a quarter-wavelength of the operating frequency when they satisfy the following expression:

$$L_s^2 = \frac{1}{4f_0}\frac{\beta_n^2}{4\pi\sqrt{3}} W_s \sqrt{\frac{E}{\rho}} \quad (14)$$

where W_s and L_s are the width and length of the support beams respectively, β_n = 4.730, 7.853, 10.996 for the first three modes of a clamped-clamped beam and f_0 is the resonance frequency of the microresonator. Figure 8 presents resonant frequency of the proposed square frame resonator versus support beam length, showing a clear increase in the resonance frequency with decreasing support length before it corresponds to around a half wavelength (λ/2) of resonant frequency of the microresonator (i.e. in this case, length of support beam virtually will be equal to zero. Thus, it causes an increase in frequency).

The performed simulations by FEA using ANSYS show that at those frequencies which resonator resonates at the fundamental mode, the support length corresponding to a quarter wavelength (λ/4) will be around 5.25 μm, which is in close agreement with Eq. 14.

Estimating quality factor: The mechanical quality factor (Q) of a resonator is:

$$Q = 2\pi\frac{W}{\Delta W} \quad (15)$$

where ΔW denotes the energy dissipated per cycle of vibration and W denotes the maximum vibration energy stored per cycle.

Many dissipation mechanisms exist in microelectromechanical resonators, such as air damping, thermoelastic damping (TED), surface loss and support loss. Unloaded Q of a microresonator is mainly the combination of these dissipation mechanisms, expressed as [4]:

$$\frac{1}{Q} = \frac{1}{Q_{air}} + \frac{1}{Q_{TED}} + \frac{1}{Q_{Surface}} + \frac{1}{Q_{Support}} \quad (16)$$

Thus, to determine Q of the designed resonator, it was necessary to calculate Q of each dissipation mechanisms as following:

Q_{air} denotes the quality factor due to energy loss mechanisms of air damping and is determined as follows:

$$Q_{air} = \frac{k}{\omega_0 b} \quad (17)$$

where k is stiffness of vibrating spring and b is damping coefficient of a rectangular parallel-plate geometries and has been derived from a linearized form of the compressible Reynolds gas-film equation as follows [13]:

$$b = \frac{3}{2\pi}\mu\frac{A^2}{d_0^3} \quad (18)$$

where $\mu = 1.78\times10^{-5}$ kg/m.s (for air in STP conditions) is coefficient of viscosity and proportional to gas pressure and consequently mean free path of gas molecules. A and d_0 are area of the device and gap between the two plates, respectively.

Q_{TED} denotes the quality factor due to energy loss mechanisms of thermoelastic damping and is expressed as [14]:

$$Q_{TED}^{-1} = \frac{E\alpha_T^2 T_0}{C_p}\frac{\omega\tau}{1+(\omega\tau)^2} \quad , \quad \tau = \frac{C_p W_r^2}{C_T \pi^2} \quad (19)$$

where α_T and C_p denote thermal expansion coefficient and specific heat at constant pressure of the material

used for the beam, respectively; T_0 is the environmental temperature and where C_T denotes thermal conductivity of the beam material and ω denotes the angular frequency of the beam resonator.

$Q_{Surface}$ denotes the quality factor due to energy loss mechanisms of surface loss and the following expression it has been suggested for it [14]:

$$Q_{Surface} = \frac{W_r h_r}{3W_r + h_r} \frac{E}{2E_{ds}\delta} \quad (20)$$

where δ denotes the characterized thickness of the surface layer and E_{ds} is a constant related to the surface stress.

$Q_{Support}$ denotes the quality factor due to energy loss mechanisms of support loss and it can be calculated as follows:

$$Q_{Support} = 2\pi \frac{KE_{tot}}{E_{loss}} \quad (21)$$

where KE_{tot} is the stored flexural vibration energy for each resonant mode of a beam resonator can be expressed as:

$$KE_{tot} = \frac{1}{2} mv^2 = \frac{1}{2} \rho h W_r L_r \omega_0^2 U_0^2 \quad (22)$$

where ω_0 and U_0 denote the fundamental angular frequency of the vibration and the vibration amplitude, respectively and E_{loss} is the energy dissipated per cycle of vibration through supports via anchors to substrate and for a clamped-free beam is calculated as follows [14]:

$$E_{loss} = \frac{1.3441+\upsilon}{Eh} \frac{}{1-\upsilon} \Gamma_0^2 \quad (23)$$

where υ is Poisson ratio of the support material and Γ_0 is a fundamental vibrating shear force on support where attached to substrate, which can be achievable by finite element analysis.

A plot of simulated quality factor versus support beam length for the proposed 72 MHz square frame resonator is shown in Fig. 9. As illustrated in the figure, the quality factor decreases rapidly below 1800 for support beams shorter than 2 μm and it is almost constant around 16000 for beams longer than 4 μm.

Figure 10 presents a comparison of quality factor versus electrode-to-resonator gap spacing between the proposed resonator and a clamped-clamped (CC) beam resonator vibrating at the fundamental flexural-mode

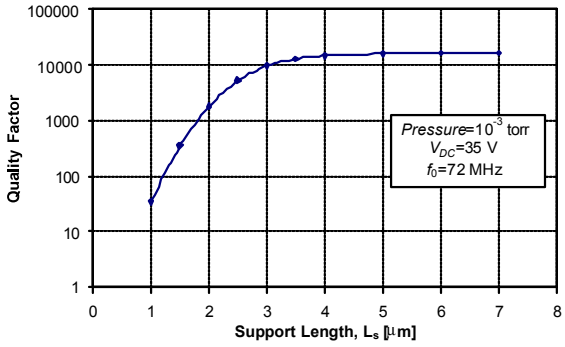

Fig. 9: Simulated quality factor versus support length plot for the 72 MHz square frame resonator

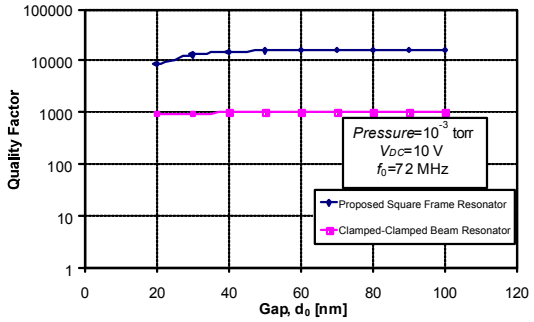

Fig. 10: Plot of Q versus electrode-to-resonator gap for the proposed and a CC beam resonator

resonant frequency. As illustrated in the figure, quality factor of the CC beam resonator is about one order of magnitude smaller than that of the square frame resonator; which is due to decrease in $Q_{Support}$ of CC beam resonator at higher frequencies. i.e., at the VHF frequencies (work frequencies of the present filter), energy loss mechanisms of support loss is dominated and has the most effect on Q_{total} of the resonator. So, as shown in Fig, 10, quality factor is independent from electrode-to-resonator gap spacing. To have a fair comparison, resonant frequency of the proposed and CC beam resonators are chosen equal to each other by proper choice of their dimensions. However, in case of square frame resonator, kinetic energy of the resonator is transferred to the anchors via four support beams which are attached to ideally motionless corners of the resonating frame. Specially, nodal points of the frame are directly available through truncating the frame corners. So, motions of the four tethers are minimized. Furthermore, energy losses to anchors via support beams are further decreased by selecting the beams corresponds to a quarter-wavelength of the resonance frequency. As a result, as shown in the figure, the square frame resonator presents a higher quality factor.

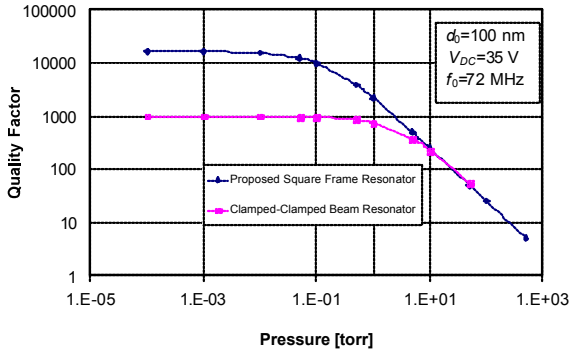

Fig. 11: Plot of Q versus ambient pressure of the microresonator

A comparison of quality factor versus ambient pressure between the proposed microresonator and a CC beam resonator vibrating at the same frequency is shown in Fig. 11. Quality factor of the proposed resonator presents one order of magnitude higher than that of the CC beam resonator, which is primarily due to higher stiffness of each constituent beam of the square frame resonator to that of the CC beam resonator.

Coupling beam design: As described earlier, two constituent resonators of the filter are designed to have the same resonance frequency. Thus, it is assumed that the passband of the overall filter is centered around this frequency. The coupling spring acts to effectively pull the resonator frequencies apart, creating two closely-spaced resonance modes that constitute the ends of the filter passband. Since in each resonance mode, the coupling beam adopts a specific shape, it is logical to consider different values for mechanical stiffness for each mode. Consequently, the frequency of each resonance peak can be calculated as follows:

$$f_1 \approx f_0\left(1-\frac{k_{c1}}{k_{rc}}\right) \quad , \quad f_2 \approx f_0\left(1+\frac{k_{c2}}{k_{rc}}\right) \tag{24}$$

where k_{rc} is the resonator stiffness at the coupling location and k_{c1} and k_{c2} are stiffness of the coupling beam at the two desired resonance modes.

The transmission band between two peaks was calculated by:

$$P.S. = f_2 - f_1 = f_0\left(\frac{k_{c2}+k_{c1}}{k_{rc}}\right) \tag{25}$$

and bandwidth of the filter can be obtained from:

$$B = \frac{P.S.}{k_{12}} \tag{26}$$

where *P.S.* is separation between the two peaks of resonance modes achieved by modal analysis using FEA and k_{12} is the normalized coupling coefficient between two resonators for a given filter type (i.e., Butterworth, Chebyshev, etc.) [15]. The needed value of coupling spring constants k_{c1} and k_{c2} was then obtained by proper choice of coupling beam geometry using expressions which will be followed.

The mechanical impedance behavior of the coupling beam as seen by the adjacent (attached) resonators for two cases of resonance mode can be conveniently modeled by the following considerations:

The resonators vibrate in-phase in the higher frequency mode and the coupling beam is in the form shown in Fig. 12(a). The mechanical impedance and stiffness of the beam are [16]:

$$Z_{c1} = \frac{f_1}{v_1} = -\frac{EI_c\alpha^3 H_6}{j\omega L_c^3 H_3} \tag{27}$$

$$k_{c1} = -\frac{EI_c\alpha^3 H_6}{L_c^3 H_3} \tag{28}$$

The resonators vibrate 180 degrees out-of-phase in the lower frequency mode and coupling beam adopts the shape which is shown in Fig. 12(b). Thus, the mechanical impedance and stiffness of the coupling beam was calculated via relations as follows [17]:

$$Z_{c2} = \frac{f_2}{v_1} = -\frac{EI_c\alpha^3 H_7}{j\omega L_c^3 H_3} \tag{29}$$

$$k_{c2} = -\frac{EI_c\alpha^3 H_7}{L_c^3 H_3} \tag{30}$$

where

$$\begin{aligned} H_1 &= \sinh\alpha\sin\alpha \\ H_3 &= \cosh\alpha\cos\alpha - 1 \\ H_6 &= \sinh\alpha\cos\alpha + \cosh\alpha\sin\alpha \\ H_7 &= \sin\alpha + \sinh\alpha \end{aligned} \tag{31}$$

and

$$\alpha = L_c(\rho W_c h_c \omega^2/(EI_c))^{0.25} \tag{32}$$

$$I_c = h_c W_c^3/12 \tag{33}$$

In order to minimize susceptibility to beam geometric variations (i.e., mass variations) caused by

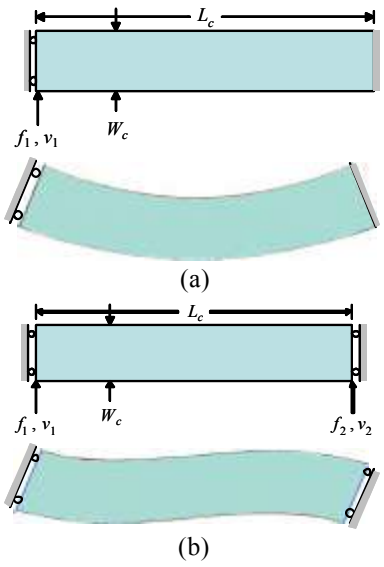

Fig. 12: Coupling beam under forces f_1 and f_2 with corresponding velocity responses at (a) 180 degrees out of and (b) in phase resonance mode

finite layout or fabrication tolerances, the coupling beam was designed to correspond to a quarter-wavelength of the filter center frequency. This was achieved by choosing $H_6 = 0$. Using the selected value of W_c and assuming that h_c is determined by the desired bandwidth of the filter, $H_6 = 0$ was solved for the L_c that corresponded to an effective quarter-wavelength of the operating frequency. The stiffnesses of a quarter-wavelength coupling beam for two indicated cases are found to be:

$$K_{c1} = 0 \quad (34)$$

and

$$k_{c2} = -\frac{EI_c\alpha^3(\sin\alpha + \sinh\alpha)}{L_c^3(\cos\alpha\cosh\alpha - 1)} \quad (35)$$

As described in Eqs. 25 and 26, peak separation (i.e. bandwidth) of the filter is directly proportional to addition of coupling spring constants k_{c1} and k_{c2} at two physical mode shapes shown in Fig. 12. Since stiffness of a flexural mode beam is related to beam dimensions, bandwidth of the filter can be set by proper choice of the coupling beam thickness (assuming beam width is dictated by lithographic and etch resolutions). Fig. 13 presents peak separation of the filter versus coupling beam thickness, showing decrease in thickness is translated to lower stiffness and lower bandwidth as a result.

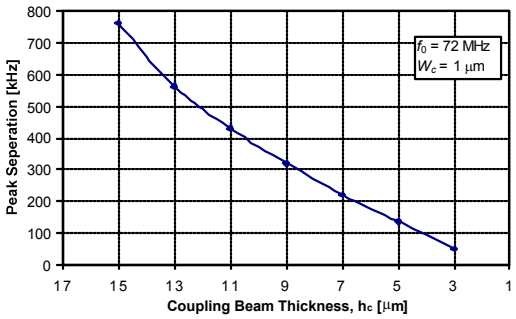

Fig. 13: Peak separation of the proposed filter versus coupling beam thickness

Micromechanical filter termination: In addition to determining the center frequency of the filter, the resonator design also dictates the termination resistors required for passband flattening. As with other type of filters, the described mechanical filters must be terminated with the proper impedance values. Without proper termination, the resonator Q's will be too large and the filter passband will consist of distinct peaks of selectivity, as seen in Fig. 2. In order to flatten the passband between the peaks, the Q's of the constituent resonators must be reduced and this can be done by terminating the filter with resistors. In Fig. 1, resistors R_{Q11}, R_{Q12}, R_{Q21} and R_{Q22} are used for this function.

The required value of total termination resistance $R_{Qi} = R_{Qi1} + R_{Qi2}$ for a mechanical filter with center frequency f_0 and bandwidth B is given by:

$$R_{Qij} = \frac{R_{xi}}{2n}\left(\frac{Q_{res}}{q_i Q_{filter}} - 1\right) \quad , \quad i = 1 \ , \ 2 \quad (36)$$

where n is the number of electrodes used in each resonator, i refers to the end resonator in question, j refers to a particular port of the end ith resonator, Q_{res} is the unloaded quality factor of the constituent resonators, $Q_{filter} = f_0/B$ and q_i is a normalized parameter obtained from a filter cookbook.[15] It is found from the Eq. (23) that the total termination resistance R_{Qi} decreases with the number of electrodes and if using the maximum capability of this design to decrease end impedances by using 8 input electrodes (4 outer electrodes and 4 inner electrodes) and 8 output electrodes (4 outer electrodes and 4 inner electrodes), the total termination impedances will be reduced by a factor of 1/8. This can be considered as an advantage for this particular configuration.

Spurious-free dynamic range: To get a measure of linearity of the filter, SFDR criterion was used.

However, before SFDR calculation, it was necessary to have an approximation about IM_3 and IIP_3 values of the filter. It must be noted that a large IIP_3 is preferred for communication applications, in general.

An expression for this IM_3 force component was obtained by approximating the beam and electrode by the lumped mass-spring-damper equivalent shown in Fig. 6 as follows:

$$F_{IM3} = V_i^3 \cdot \left\{ \frac{1}{4}\frac{(\varepsilon_0 A_0)^2}{d_0^5}\frac{V_{DC}}{k_{reff}}[2\theta_1 + \theta_2] + \frac{3}{4}\frac{(\varepsilon_0 A_0)^3}{d_0^8}\frac{V_{DC}^3}{k_{reff}^2}\theta_1[\theta_1 + 2\theta_2] + \frac{3}{2}\frac{(\varepsilon_0 A_0)^4}{d_0^{11}}\frac{V_{DC}^5}{k_{reff}^3}\theta_1^2\theta_2 \right\} \quad (37)$$

where ε_0, is the permittivity in vacuum, $A_0=W_rW_e$ is the electrode-to-resonator overlap area, $\theta_1=\theta(\omega_1)$ and $\theta_2=\theta(\omega_2)$; where:

$$\theta(\omega) = \frac{1}{1-(\omega/\omega_0)^2 + j\omega/(Q\omega_0)} \quad (38)$$

and k_{reff} is the effective integrated stiffness at the midpoint of the beam.

In the Eq. (37), static bending of the beam caused by the applied dc-bias V_{DC} was not neglected unlike the previous works [18]. By equating Eq. (37) with the fundamental force component

$$F_{fund} = V_{DC}\frac{C_0}{d_0}V_i = V_{DC}\frac{\varepsilon_0 A_0}{d_0^2}V_i \quad (39)$$

and solving the expression for V_i, the input voltage magnitude at the IIP_3 and consequently P_{IIP3} was found. Assuming the generated current in the resonator was the same current in the filter, P_{IIP3} of the filter was calculated as follows:

$$P_{i,filter} = \frac{2(R_{Qi} + R_x)}{R_x} \cdot P_{i,resonator} \quad (40)$$

The out-of-band SFDR (with tones 400 and 800 kHz offset from the filter center frequency) was determined via the expression [19]:

$$SFDR = \tfrac{2}{3}(IIP3 - kT - IL - 10\log B) - SNR_{min} \quad (41)$$

where all quantities are in decibels, SNR_{min} is the required minimum signal-to-noise ratio, k is the Boltzmann constant, T is temperature in Kelvin and kT is the thermal noise power delivered by R_Q into a matched load, IL is the insertion loss of the filter and B is the filter bandwidth. Figure 14 compares a plot of output power P_o versus input power P_i between the present and a CC beam based polysilicon microfilter, both working at the same frequency.

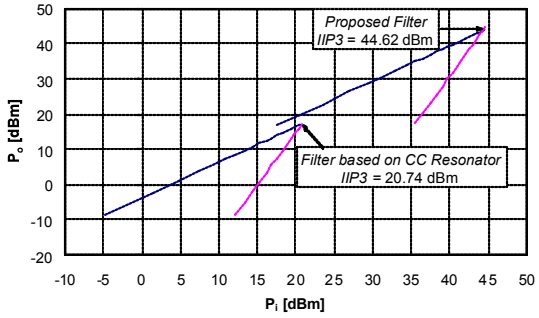

Fig. 14: Simulated output power P_o versus input power P_i plot for determination of IIP_3 for the proposed and a CC beam microresonator vibrating at the same frequency. Input tones for IM_3 determination are spaced 400 and 800 kHz from the resonator center frequency

Table 1: Material properties and surrounding conditions of the filter

Parameter	Explanation	Value	Units
E	Young's modulus for polysilicon	150	GPa
ρ	Density of polysilicon	2,300	kg/m^3
υ	Poisson's ratio	0.28	—
α_T	Thermal expansion coefficient	2.6×10^{-6}	K
C_p	Specific heat	1.63×10^{6}	J/Km^3
C_T	Thermal conductivity	90	W/mK
T_0	Environmental temperature	300	K
μ	Absolute viscosity of air	1.78×10^{-5}	Ns/m^2
P_a	Ambient pressure	0.1	torr

Micromechanical filter and resonator characteristics: The simulated spectrums for the properly terminated 72 MHz two-resonator micromechanical filter based on the proposed square frame resonator and a filter based on 72 MHz CC beam resonator are shown in Fig. 15. The bandwidths of the filters are around 285 kHz. Thanks to the higher quality factor, the insertion loss for the proposed filter is only 0.44 dB and calculated via the following formula:

$$IL = 20\log\left(\frac{R_Q + R_x}{R_Q}\right) \quad (42)$$

Table 2: Micromechanical resonator characteristics

Parameter	Explanation Value	Units	
f_0	Mechanical resonance frequency	72.7	MHz
κ	Frequency modification factor	0.99274	-
L_r	Average beam length	10	µm
W_r	Beam width	2	µm
h_r	Structural thickness	15	µm
W_e(out)	Outer electrode width	5	µm
W_e(in)	Inner electrode width	4	µm
d_0	Electrode to res. gap	100	nm
L_s	Support beam length	5.3	µm
W_s	Support beam width	1	µm
h_s	Support beam thickness	15	µm
Q	Quality factor	9,912	-
m_r	Resonator mass at middle of each beam	3.45×10^{-13}	kg
k_{mech}	Resonator stiffness at middle of each beam	72,000	N/m
k_{elec}	Electrical spring constant	-1255	N/m
η_e	Transduction parameter	2.228×10^{-6}	C/m
V_{DC}	DC-Bias voltage	35	V
R_x	Motional resistance	478	Ω

Table 3: Calculated Q of each dissipation mechanisms and total Q of the resonator

Q_{air}	Q_{TED}	$Q_{Surface}$	$Q_{Support}$	Q_{total}
24,955	19,500	126,050	625,572	9,912

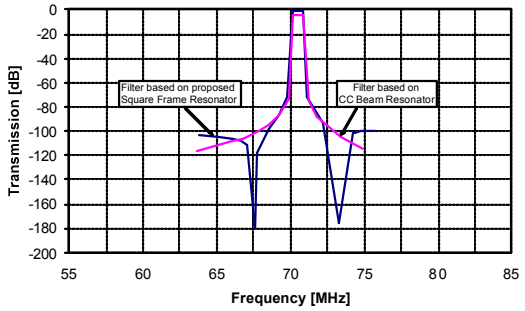

Fig. 15: Mechanical frequency response of the designed filter without applying *dc*-bias voltage V_{DC}

Eq. (42) calculates that insertion loss of a 72 MHz filter based on CC beam resonator is almost 6 dB.

The material properties used in this work and surrounding conditions of the filter are listed in Table 1. Table 2 lists the simulated micromechanical resonator summary. The calculated quality factor of the resonator and each of dissipation mechanisms are presented in Table 3. Finally, Table 4 lists the present micromechanical filter characteristics.

Table 4: IF Micromechanical filter summary

Parameter	Explanation	Value	Units
L_c	Coupling beam length	5.3	µm
W_c	Coupling beam width	1	µm
h_c	Coupling beam thickness	6	µm
f_0	Center frequency	72	MHz
P.S.	Peak seperation	206	kHz
B	3dB bandwidth	285	kHz
Q	Quality factor	250	-
I.L.	Insertion loss	0.44	dB
SFDR	Spurious free dynamic range	~99	dB
R_{Qi}	Q-control resistors	9	kΩ

CONCLUSION

Design and simulation of an IF micromechanical filter based on the new structure square frame microresonator suitable for operating around 72 MHz was reported. The proposed microresonator exhibits series motional resistances considerably smaller than that of other beam resonators by a factor equal to the number of electrodes used in each resonator. The present method for R_x-reduction does not degrade linearity of the resonator and in contrast to arrayed microresonators, does not consume extra chip area. This technique alleviates some of remaining challenges that slow the advancement in integration resonators, filters and oscillators into communication systems and helps to realizing a single-chip, fully integrated communication system based on RF MEMS technology.

ACKNOWLEDGMENT

The research grant given by Iran Telecommunication Research Center (ITRC) for the support of this work is highly appreciated.

REFERENCES

1. Nguyen, C.T.-C., 1998. Microelectromechanical Devices for Wireless Communications. In: The Eleventh Annual International Workshop on Micro Electro Mechanical Systems. Heidelberg, Germany, 25-29 January 1998. IEEE Press, pp: 1-7.
2. Nguyen, C.T.-C., 1999. Frequency-Selective MEMS for Miniaturized Low-Power Communication Devices. IEEE T. Microw. Theory, 47: 1486-1503.

3. De Los Santos, H.J., 2002. RF MEMS Circuit Design for Wireless Communications. 1st Edn., Artech House, Boston.
4. Bannon III, F.D., J.R. Clark and C.T.-C. Nguyen, 2000. High-Q HF Microelectromechanical Filters. IEEE J. Solid-St Circ., 35: 512-526.
5. Demirci, M.U., M.A. Abdelmoneum and C.T.-C. Nguyen, 2003. Mechanically Corner-Coupled Square Microresonator Array for Reduced Series Motional Resistance. In: The 12th International Conference on Solid-State Sensors, Actuators and Microsystems. Boston, Massachusetts, USA, 8-12 June 2003. IEEE Press, pp: 955-958.
6. Navid, R., J.R. Clark, M. Demirci and C.T.-C. Nguyen, 2001. Third-order intermodulation distortion capacitively-driven CC-beam micromechanical resonators. In: The 14th IEEE International Conference on Micro Electro Mechanical Systems. Interlaken, Switzerland, 21-25 January 2001. IEEE Press, pp: 228-231.
7. Alastalo, A.T. and V. Kaajakari, 2006. Third-Order Intermodulation in Microelectromechanical Filters Coupled With Capacitive Transducers. J. Microelectromech. S., 15: 141-148.
8. Varadan, V.K. and K.J. Vinoy, 2002. RF MEMS and their Applications. 1st Edn., John Wiley and Sons.
9. Wang, K., A.-C. Wong and C.T.-C. Nguyen, 2000. VHF Free-Free Beam High-Q Micromechanical Resonators. J. Microelectromech. S., 9: 347-360.
10. Timoshenko, S., D.H. Young and W. Weaver, 1974. Vibration Problems in Engineering. 4th Edn. John Wiley and Sons, New York.
11. Nathanson, H.C., W.E. Newell, R.A. Wickstrom and J.R.Jr., Davis, 1967. The Resonant Gate Transistor. IEEE T. Electron Dev., ED-14: 117-133.
12. Elwenspoek, M. and R. Wiegerink, 2001. Mechanical Microsensors. 1st Edn., Springer-Verlag.
13. Rebeiz, G.M., 2003. RF MEMS: Theory, Design and Technology. 1st Edn., John Wiley and Sons, New Jersey.
14. Hao, Z., A. Erbil and F. Ayazi, 2003. An analytical model for support loss in micromachined beam resonators with in-plane flexural vibrations. Sensor. Actuat. A-Phys., 109: 156-164.
15. Zverev, A.I., 2005. Handbook of Filter Synthesis. 2nd Edn., John Wiley and Sons, New York.
16. Konno, M., S. Oyama and Y. Tomikawa, 1979. IEEE T. Sonics and Ultrasonics, SU-26: 191-201.
17. Johnson, R.A., 1971. Mechanical Filters-A Review of Progress. IEEE T. Sonics and Ultrasonics, SU-18: 155-170.
18. Bannon III, F.D., J.R. Clark and C.T.-C. Nguyen, 1996. High frequency microelectromechanical IF Filters. In: International Electron Devices Meeting. San Francisco, California, USA, 8-11 December 1996. IEEE Press, pp: 773-776.
19. Razavi, B., 1998. RF Microelectronics. 1st Edn., Prentice Hall PTR, New Jersey.